Measurement of the spin of the M87 black hole from its observed twisted light

Fabrizio Tamburini,[1,*] Bo Thidé,[2,†] and Massimo Della Valle[3,‡]

[1]*ZKM, Lorenzstrasse 19, Karlsruhe, D-76135 Germany*
[2]*Swedish Institute of Space Physics, Ångström Laboratory, Box 537, SE-751 21 Uppsala, Sweden*
[3]*Capodimonte Astronomical Observatory, INAF-Napoli,*
Salita Moiariello Naples Salita Moiariello 16, I-80131 Napoli, Italy

The warped spacetime around a black hole modifies the propagation of light and radio. A recent study predicted that light emitted from the immediate vicinity of a massive rotating black hole (BH) should be twisted [1], *i.e.* be imprinted with orbital angular momentum (OAM) [2]. This vorticity, caused by general relativity (GR) effects such as spacetime dragging and mixing, and gravitational lensing, enables new ways to study BH's, including their rotation, and to test fundamental properties of GR itself. Here we report the detection of GR induced vorticity [1] in radio emitted from the Einstein ring surrounding the shadow of the rotating $\sim 6.5\times10^9$ solar mass BH in the core of the M87 galaxy, as observed by the Event Horizon Telescope (EHT) [3–6]. The M87 spiral spectra [7] were identified in EHT intensity profile data by using a wavefront reconstruction technique [8] enabling the recovery of the phase front [9]. They reveal that the M87 BH rotates clockwise, with inclination $i = 17^\circ$ and rotation parameter $a \sim 0.9 \pm 0.1$, corresponding to a rotational energy [10] of about 10^{64} erg. Our findings agree with published constraints [11] and with analysis of the amplitude and phase profiles in fiducial pipeline images released by the EHT collaboration [4]. Using structured light [12, 13] to make the first direct measurement of Kerr metrics and to reveal one of the most energetic astrophysical phenomenon ever observed, corresponding to the energy radiated by the brightest quasars over Gyr timescales, is a breakthrough that is likely to invigorate BH research and open new perspectives in astronomy and astrophysics.

I. INTRODUCTION

Most of the knowledge we have about our Universe has been gained by the observation and interpretation of electromagnetic (EM) radiation. This ranges from visible light caught by the naked eye, to radio and light emissions intercepted by advanced telescopes. One example of the latter is the concerted international radio astronomy effort Event Horizon Telescope (EHT) that has produced breakthrough results by observing the central compact radio source that surrounds a supermassive black hole in the Virgo Cluster galaxy M87 [3–6].

Radio/optical astronomy relies on the fact that electromagnetic radiation carries energy and linear momentum, manifesting itself in translational force action and radiation pressure. However, EM radiation can also carry angular momentum connected with rotation and torque action [2]. These observables, plus the centre of energy vector of the field, form a set of ten conserved quantities, concomitant with the ten-dimensional Poincaré group of Noether invariants. In fact, the Poincaré set itself is a subset of a much larger set of conserved quantities in Maxwell's electrodynamics [14], a set that includes supertranslation and superrotation of spacetime and EM fields [15]. Information is encoded, naturally or artificially, into these conserved EM observables and transported by them from the source to the distant observer where the information is decoded and recovered. Clearly, not making use of all observables carried by the EM field is not extracting all information present in the radio and light emitted by a source.

Up to now, the EM radiation quantities exploited in observational astronomy have been limited to a subset of the ten Noether invariants carried by the EM field, *viz.* the energy, the linear momentum, and the wave polarization, *i.e.* the spin angular momentum (SAM) $\mathbf{S}$ associated with photon helicity. This subset can be extended by making full use of the total angular momentum $\mathbf{J} = \mathbf{S} + \mathbf{L}$, where $\mathbf{L}$ is the orbital angular momentum (OAM) [16, 17]. Unlike $\mathbf{S}$ and $\mathbf{L}$ separately, their (pseudo)vectorial sum $\mathbf{J}$ is an invariant, and hence always conserved in a closed system. The translational (linear momentum) as well as the rotational (angular momentum) properties of the EM field remain valid down to the single photon level [18, 19], a fact that is further substantiated in the Majorana photon wavefunction formalism [17, 20] with its complete equivalence to quantum electrodynamics [21].

In a theoretical analysis, supported by numerical simulations and computer modelling of twisted light from near the SgrA* Kerr BH, performed by Tamburini *et al.* [1], it was claimed that the utilization of structured light and OAM in observational astronomy may provide new, unique tools to identify and study black holes, determine their rotational state, and to test hitherto untested aspects of general relativity (GR). The results reported here support these claims.

Benefitting from the fact that Earth and M87 are in relative motion, we were able to recreate the phase front from an analysis, with a Transport of Intensity Equation (TIE) method [8, 9], of the intensity of the 1.3 mm radiation emitted from the M87 Einstein ring around the black hole. This allowed us to obtain the OAM spectrum (spiral spectrum) of the received radio light, thus confirming the predictions made in Ref. 1. Furthermore, from the asymmetry of the observed OAM we were able to determine the sense and magnitude of the rotation of the M87 black hole and its inclination.

* Electronic address: fabrizio.tamburini@gmail.com
† Electronic address: bt@irfu.se
‡ Electronic address: massimo.dellavalle@inaf.it

Table I. **Asymmetry ratio from numerical simulations.**

BH rotation parameter a	0.5	0.6	0.8	0.9
Asymmetry ratio $q = h(m=1)/h(m=-1)$				
$i = 17^\circ$	1.295	1.320	1.356	1.391
$i = 46^\circ$	1.392	1.412	1.424	1.438

Simulation of the asymmetry parameter q of Kerr black holes with different rotation parameters $0.5 < a < 0.9$ and inclinations $i = 17^\circ$ and $i = 46^\circ$. The rotation is clockwise, the spin of the black hole is pointing away from the Earth (see text). The parameter q is obtained by dividing the height of the $m = 1$ component, $h(m = 1)$ by that of $m = -1$, $h(m = -1)$ present in each spiral spectrum. In the numerical simulations here reported, $q > 1$ that indicates a clockwise rotation ($q = 1$ indicates no rotation and $q < 1$ counterclockwise rotation).

II. RESULTS

Superpositions of photon eigenstates, each with a well-defined value $\sigma\hbar$ of spin angular momentum and $m\hbar$ of orbital angular momentum [22], are formed near a rotating black hole due to the dragging of light in Kerr spacetime [1]. The Einstein ring surrounding the shadow of the black hole is created by such lensed beams, experiencing an anamorphic transformation [23] that is accompanied by a polarization rotation [24] due to the gravitational Faraday effect [25], image deformation, and rotation due to the lensing of the curved spacetime as well as other modifications in the phase wavefront, including gravitational Berry phase effects [26–28]. Light propagating near rotating black holes experiences a behaviour that is analogous to that in an inhomogeneous anisotropic medium in a mechanism related to the Pancharatnam-Berry geometrical phase that involves spatially inhomogeneous transformations of the polarization vector in the observation plane of an asymptotic observer. Being the radio source in the M87 galaxy resolved by the EHT baseline, the wavefront is obviously not plane such as that emitted from a point-like source at infinity, even if the distance from the source to the Earth is $D = 16.8$ Mpc. Thus we can determine, with good approximation, the OAM content in the wavefront with the methods used here.

The evolution of the M87 Einstein ring structure during the two different observation runs (epoch 1 and epoch 2) of EHT in two 2 GHz frequency bands centred on 227.1 GHz and 229.1 GHz (for more details see Ref. 6), each separated by one day, is negligible and can be taken as evidence that only higher-order, small perturbations are present in the spiral spectrum. In fact, observations confirm that the EHT 2017 data has tracks from four separate days of observing and, relative to the object, each day is $2.8R_g c^{-1}$ long for a BH with mass [6] $M = 6.5 \pm 0.2|_{\rm stat} \pm 0.7|_{\rm sys} \times 10^9\, M_\odot$. This timescale is smaller than the crossing time of light of the source plasma and short compared to the decorrelation timescale of EHT simulations used to analyze the experimental results [5], $50R_g c^{-1}$.

This is the reason why we chose to estimate the OAM from the asymmetry parameter q of the OAM spectrum components $m = 1$ and $m = -1$ only. If $q > 1$, then the rotation is clockwise, whilst $q = 1$ indicates no rotation [2]. The rotation parameter, a, can be calculated from the asymmetries present in the experimental and theoretical spiral spectra. The value of a was estimated from the experimental data from two different runs, each separated by one day, the first being epoch 1 (April 5 and 6, 2017, respectively), and the second being epoch 2 (April 10 and 11, 2017). The data were obtained from 10 seconds of signal averaging as described in Refs. 4–6. The imaging techniques applied to this data set reveal the presence of an asymmetric ring with clockwise rotation and a "crescent" geometric structure that exhibits a clear central brightness depression. This indicates a source dominated by lensed emission surrounding the black hole shadow.

From the analysis of the two data sets we obtain the asymmetry parameters $q_1 = 1.417$ for epoch 1 and $q_2 = 1.369$ for epoch 2. They give an averaged asymmetry in the spiral spectrum of $\overline{q} = 1.393 \pm 0.024$ in agreement with that of our numerical simulations, $q_{\rm num} = 1.375$, of partially incoherent light emitted by the Einstein ring of a Kerr black hole with $a \sim 0.9 \pm 0.1$, corresponding to a rotational energy [10] of 10^{64} erg, which is comparable to the energy radiated by the brightest quasars over a Gyr timescale, and inclination $i = 17^\circ$ between the approaching jet and the line of sight, with the angular momenta of the accretion flow and of the black hole anti-aligned, showing clockwise rotation as described in Ref. 5.

This result is in good agreement with results from the analysis of the fiducial pipeline images of amplitude and phase plots for 11 April, 2017 of DIFMAP with $q = 1.401$, EHT $q = 1.361$ and SMILI, $q = 1.319$, [6] giving for that day an averaged value $\overline{q} = 1.360$ that deviates of 0.09 from epoch 2 value estimated with TIE and $q > 0$ confirm the clockwise rotation. The spiral spectra are reported in Fig. 2.

Then one determines the rotation parameter a by comparing those obtained by a linear interpolation with the asymmetry parameter q of various models, as reported in the numerical example of Table I for different values of inclination and rotation parameters i and q. The results are depicted in Fig. 1.

In our simulations we adopted a thermalized emission with $0.1 < \Gamma < 2$ power spectra, chosen in agreement with ALMA observations [5, 30] and also that of a synchrotron emission, Compton scattering, and bremsstrahlung. We find that in any case, as discussed in Ref. 6, the image is determined mainly by the spacetime geometry and is also insensitive to the details of the plasma evolution between each observation in each of the two epochs.

Even if this is not a direct measure of the spatial phase profile, something that could be obtained with interferometric or other more direct techniques, the values of the rotation parameter a obtained with this method agrees with the experimental data obtained from the results present in the literature. Preferably, one should have several snapshots taken with EHT at much shorter time intervals, typically a few minutes rather than days. This would improve the terms present in the TIE of Eqns. (A8), and could be realized quite straightforwardly.

With dedicated observations and new fiducial pipeline images of amplitude and phase plots, and new interferometric methods that analyze the EM field in intensity and phase, readily realized with standard radio telescopes as was reported for

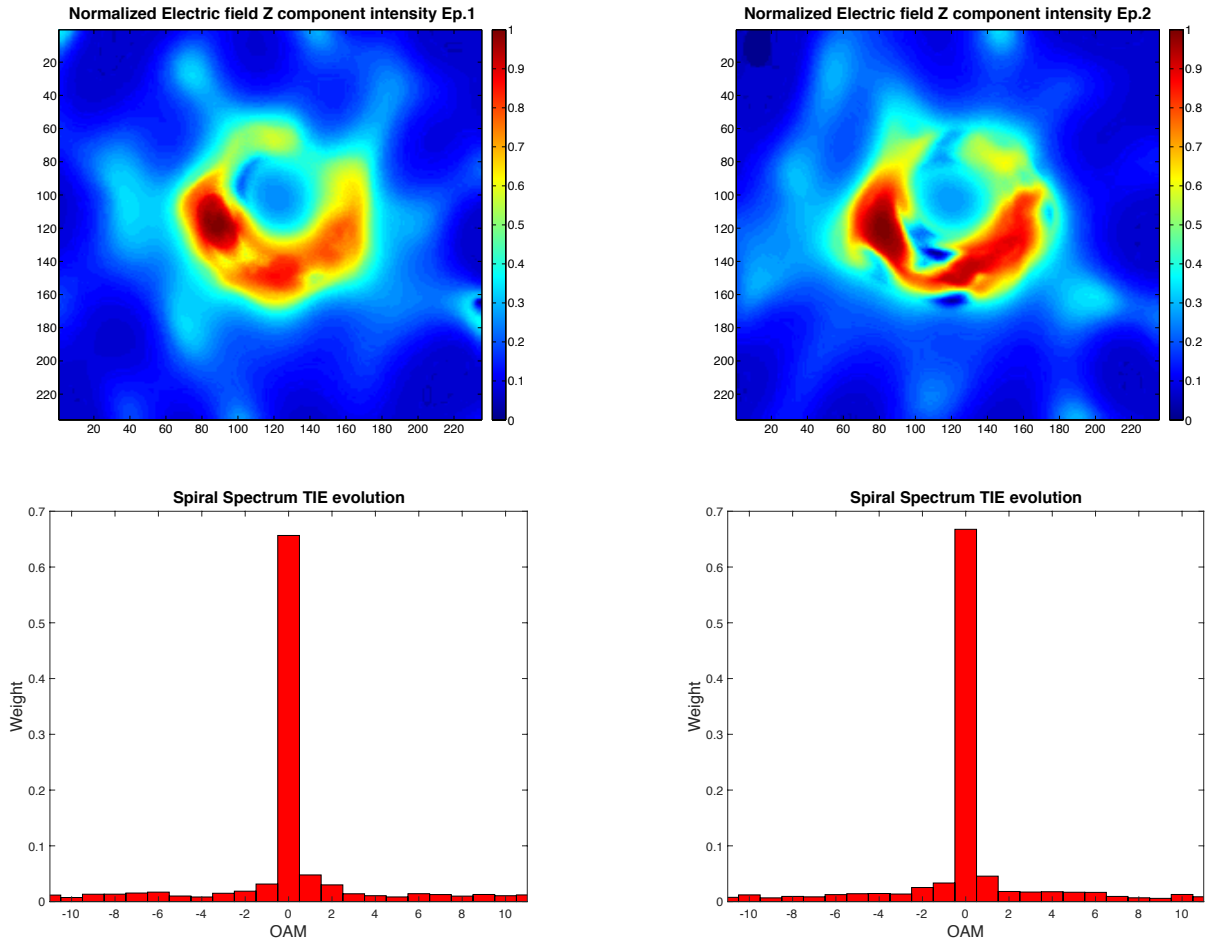

Figure 1. **Experimental results.** Field components along the observer's direction and spiral spectra obtained with the TIE method for epoch 1 and epoch 2. The asymmetry between the $m = 1$ and $m = -1$ components in both of the spiral spectra reveals the rotation of the black hole in M87. It also indicates that the electromagnetic vortex reconstructed from the TIE analysis of the EM field intensities extracted from the birghtness temperature in a finite frequency bandwidth has components along the propagation direction to the observer that are compatible with twisted lensing of a black hole with $a = 0.9 \pm 0.1$ rotating clockwise with the spin pointing away from Earth and an Einstein ring with a gravitational radius $R_g = 5$, as indicated by an EHT analysis dominated by incoherent emission. For all days, the diameters of the ring features span the narrow range 38–44μ-arcseconds and the observed peak brightness temperature of the ring is $T \sim 6 \times 10^9$ K.[6] The other components (x and y) of the EM field derived from TIE equations do not show a predominant OAM component. This is expected [1].

the fiducial pipeline images of amplitude and phase plots for 11 April 2017, one should be able to drastically improve the measurement of the OAM content (spiral spectrum) in the EM radiation from rotating black holes and determine much better their rotation and other parameters once the shadow is resolved. Ultimately, radio telescopes equipped with antenna systems optimized to directly capture and resolve the EM angular momentum in the signals received will be able to unleash the full potential of the OAM in observational astronomy.

The advantage of involving OAM in black hole astronomy is that polarization and OAM together build up the total angular momentum invariant **J** and when polarization is affected by the presence of polarising media such as dust and unstructured plasma, OAM will be less affected and can be used as a reference point to extract additional information about the source from its emitted light.

Appendix A: Technical

In the paraxial approximation applicable here, it is possible to split the total angular momentum **J** into two distinct gauge-invariant observables **S** and **L**, thus allowing them to be studied separately [31]. In this case, one can project **S** and **L** onto the propagation axis z to obtain two distinct and commuting operators [17]

$$\hat{S}_z = \hbar \sum_{\sigma,m,p} \sigma \int_0^\infty \mathrm{d}k_0 \hat{a}^\dagger_{\sigma,m,p}(k_0)\hat{a}_{\sigma,m,p}(k_0) \tag{A1a}$$

$$\hat{L}_z = \hbar \sum_{\sigma,m,p} m \int_0^\infty \mathrm{d}k_0 \hat{a}^\dagger_{\sigma,m,p}(k_0)\hat{a}_{\sigma,m,p}(k_0) \tag{A1b}$$

where $\hat{a}_{\sigma,m,p}(k_0)$ and $\hat{a}^\dagger_{\sigma,m,p}(k_0)$ are the creation/annihilation operators of the EM field, characterized by the spin

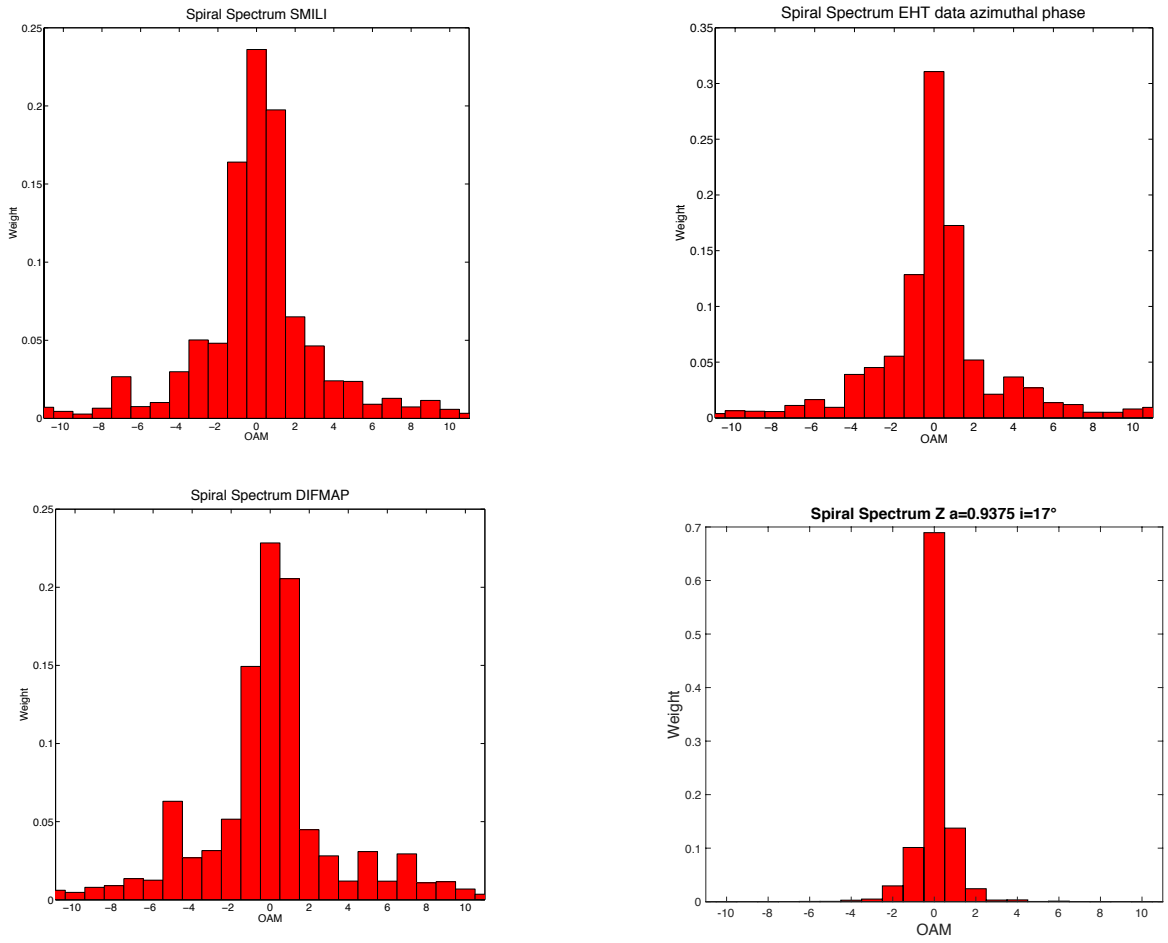

Figure 2. **Results from DIFMAP, EHT and SMILI data analyses and of numerical simulations from KERTAP.** *The first three insets* show the experimental spiral spectra obtained from the three fiducial pipeline images for 11 April 2017 from SMILI, EHT imaging, and DIFMAP [4]. They represent the visibility amplitude and phase as a function of the vector baseline. In all the datasets the asymmetry parameter, the ratio between the $m = 1$ and $m = -1$ peaks in the spiral spectra, is $q > 1$ indicating clockwise rotation: the black hole is found to have its spin pointing away from Earth and an inclination between the approaching jet and the line of sight of $i = 17^\circ$ (equivalent to a similar geometry with an inclination $i = 163^\circ$, but where the angular momentum of the accretion flow and that of the BH are anti-aligned) (*left*). *Fourth inset:* spiral spectrum of the numerical simulations with KERTAP [29] obtained from the normalized intensity and phase of the z component of the radiation field emitted from a spatially resolved image of the black hole accretion disc dominated by thermalized emission with $\Gamma = 2$. The coherence χ of the radiation emission is characterized by the ratio between the $m = 0$ and $m = 1$ peaks in the spiral spectra. The lower the χ, the higher the coherence in the emission. The experimental spiral spectra of SMILI, EHT imaging, and DIFMAP show higher coherence in the radiation emission ($\chi_{\rm SMILI} = 1.198$, $\chi_{\rm EHT} = 1.798$) and ($\chi_{\rm DIFMAP} = 1.107$) with respect to the simulated model of a simple thermalized accretion disk with power spectrum $\Gamma = 2$ ($\chi_{\rm KERTAP} = 5.029$) and with respect to that obtained in the TIE reconstruction of the wavefront ($\chi_{\rm ep1} = 13.745$ and $\chi_{\rm ep2} = 14.649$) in Fig.1. Even if the asymmetry q is well preserved, the TIE method can be improved by consecutive data acquisitions of the wavefront, separated by a much shorter time interval than one day and might therefore provide better information on the source emission.

(σ), orbital (m) and radial (p) angular momentum states. Hence, each individual photon in the beam carries SAM, quantized as $S_z = \sigma\hbar, \sigma = \pm 1$, and OAM, quantized as $L_z = m\hbar, m = 0, \pm 1, \pm 2, \ldots, \pm N$.

Twisted beams can be decomposed into orthogonal eigenmodes, each carrying its own well-defined quantum of OAM and known geometry, such as Laguerre-Gaussian modes. In cylindrical polar coordinates (ρ, φ, z) these paraxially approximate modes describe an EM field at $z = 0$ of amplitude [32]

$$U_{m,p}{}^{\rm L\text{–}G}(r,\varphi,0) \propto \left(\frac{\sqrt{2}\rho}{w(0)}\right)^m {L_p}^m\left(\frac{2\rho^2}{w^2(0)}\right) \times \exp\left(-\frac{\rho^2}{w^2(0)}\right)\exp\left(\pm i m\varphi\right) \quad \text{(A2)}$$

The parameter m is the azimuthal index that describes the z component of OAM, *i.e.* the number of twists present in the helical wavefront, p the number of radial nodes of the mode, $w(z)$ the waist of the beam, ${L_p}^m$ the associated Laguerre orthogonal

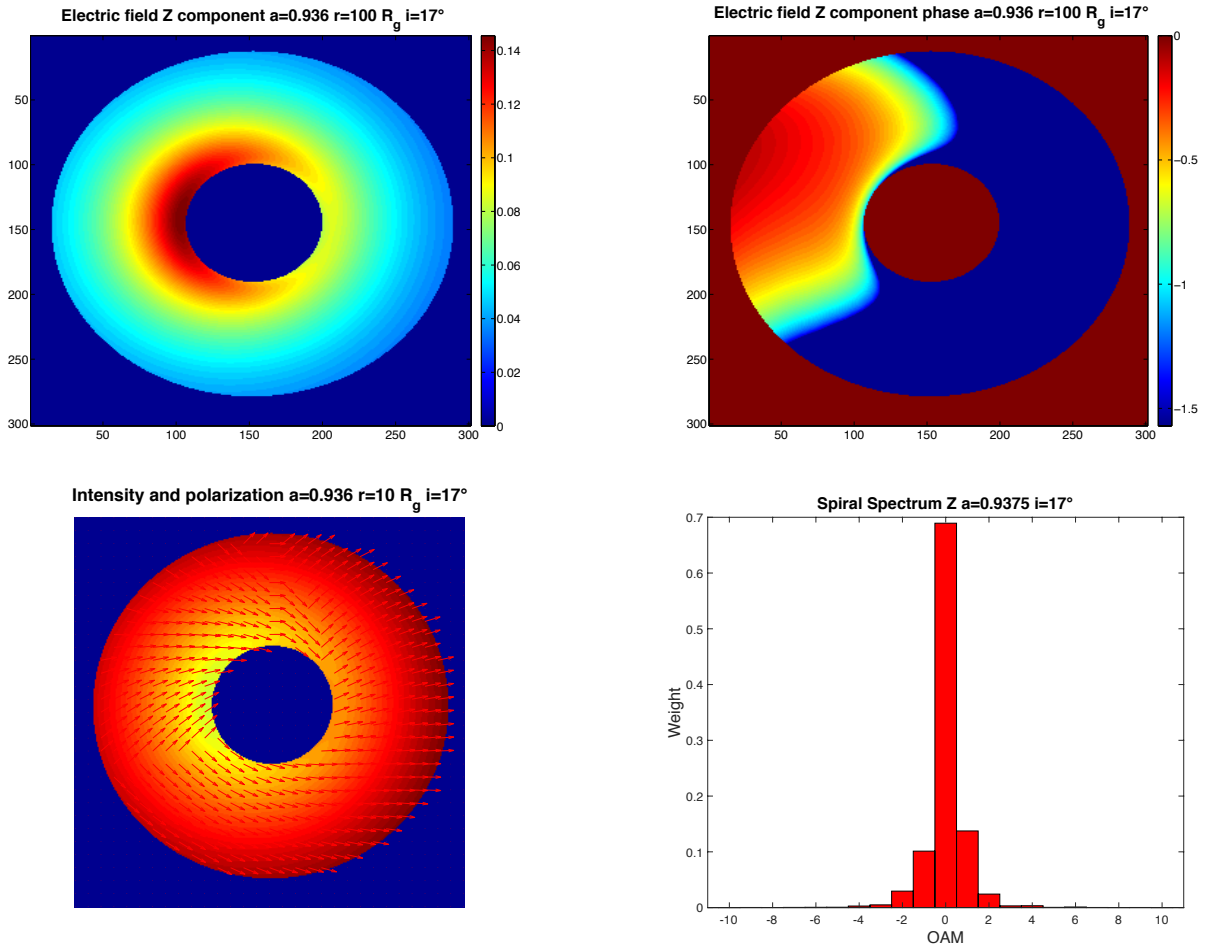

Figure 3. **Results of numerical simulations from KERTAP [29].** Normalized intensity and phase of the z component of the radiation field (upper panels) emitted from a spatially resolved image of the black hole accretion disc dominated by thermalized emission and synchrotron radiation. The black hole has a spin pointing away from Earth and an inclination between the approaching jet and the line of sight of $i = 17°$, equivalent to a similar geometry with an inclination $i = 163°$ and the angular momentum of the accretion flow is anti-aligned with that of the BH. Polarization and spiral spectrum plots (lower panels). This geometry, shown here at an orientation of 90°, agrees with that described by the experimental spiral spectra in Fig. 1 with clockwise rotation in agreement with the asymmetry parameter q. The ratio between the $m = 0$ and $m = 1$ peaks of the experimental data results smaller than that generated by the theoretical model, showing lower coherence in the emission mechanisms.

polynomial, and φ the azimuthal phase of the beam[19,20]. The decomposition of any general beam into orthogonal modes will expose the spectrum of OAM states carried by the EM wavefront, the so called spiral spectrum [7].

Numerical simulations and analyses. As an initial step in the analysis and interpretation of the data, we built up, from a set of numerical simulations, several scenarios of black-hole (BH) accretion disks (AD's) to use as a catalogue of reference models to be compared with the results from the experimental data analysis, allowing us to characterize the twisting of light from the rotating BH of M87. To this end we solved numerically the null geodesic equations under strong gravity conditions with the help of the software package KERTAP [29] that provides a detailed description of the propagation of light in Kerr spacetime in geometric units ($G = c = 1$). We calculated the OAM of light from the Stokes polarization parameters [8] as measured by an ideal asymptotic observer. Because of the properties of the Kerr metric, the observables associated with any Kerr black hole (KBH), including the spatial distribution of the azimuthal photon phase $\phi(\varphi)$ and the associated OAM spiral spectrum considered here, are invariant with respect to the mass $m_{\rm BH}$ of the BH but depend on its rotation parameter $a = J_{\rm BH}/(m_{\rm BH}c)$, where $J_{\rm BH}$ is the BH angular momentum, and the inclination i of its equatorial plane with respect to the observer. In all our simulations we assumed $0.5 < a < 0.99$ and $1° < i < 179°$, rotating clockwise and counterclockwise, then favouring $i = 17°$ rotating clockwise and pointing away from Earth (or equivalent to $i = 163°$ with the angular momentum of the accretion flow and that of the BH anti-aligned as discussed in Ref. 5), as indicated by the spiral spectra obtained from the experimental data and from the results of EHT collaboration presented and discussed in Refs. 3–6.

Employing a new vectorial field technique developed by Zhang *et al.*[8], we first calculated the Stokes parameters for an ideal BH AD with given values of a and i. We then determined the OAM of light from the Pancharatnam-Berry phase generated by the KBH lensing. For this purpose we considered the electric field of a fully polarized vectorial vortex beam propagating in free space in the z direction from the BH to the asymptotic observer. In the paraxial approximation this field can be written [*cf.* Eqn. (1.5) in Ref. 33]

$$\mathbf{E}(x,y) = \mathrm{i}\omega \left[u_x \hat{\mathbf{x}} + u_y \hat{\mathbf{y}} + \frac{\mathrm{i}}{k} \left(\frac{\partial u_x}{\partial x} + \frac{\partial u_y}{\partial y} \right) \hat{\mathbf{z}} \right] \exp(\mathrm{i}kz) \tag{A3}$$

where u_x, u_y u_x^* and u_y^* represent the complex amplitudes of the x and y components and their complex conjugates, respectively, of the electric field in the image plane, ω is the angular frequency, and k the wave number.

In SI units the z component of the EM orbital angular momentum density about the origin is [31]

$$\varepsilon_0 [\mathbf{x} \times (\mathbf{E} \times \mathbf{B})] \cdot \hat{\mathbf{z}} = \frac{\varepsilon_0}{2\omega} \sum_{i=1}^{3} E^* \hat{L}_z E_i = \frac{\varepsilon_0}{2\omega} \sum_{i=1}^{3} E_i^* \left(-\mathrm{i} \frac{\partial}{\partial \varphi} \right) E_i$$

so that one obtains [8]

$$\hat{L}_z = \mathrm{i} \frac{\omega}{2} \left(u_x \frac{\partial u_x^*}{\partial \varphi} + u_y \frac{\partial u_y^*}{\partial \varphi} - u_x^* \frac{\partial}{\partial \varphi} - u_y^* \frac{\partial}{\partial \varphi} \right) \tag{A4}$$

From the Stokes parameters (I,U,V) of the linear and elliptic states of EM polarization taken as reference fields, the Pancharatnam phase of the vortex field $\mathbf{E}(x,y)$ we want to determine is given by [8]

$$\psi_{P(V/U)} = \arg \left(\langle \Phi_V | \Phi_{\mathbf{E}} \rangle \right) \tag{A5}$$

More precisely, this quantity is calculated with the argument of the ratio between the circular/elliptic state of polarization of the EM field, characterized by the Stokes parameter V, and state $|\Phi_V\rangle$, and that of the initial field $\mathbf{E}(x,y)$, namely $|\Phi_{\mathbf{E}}\rangle$.

According to Zhang *et al.* [8], one obtains the average OAM charge of the field, for any concentric circle of pixels with the origin in the centre of the image with radius r_c, from

$$\frac{\partial m}{\partial \varphi} = r_c I_N \left(-I \frac{\partial \psi_{P(V/U)}}{\partial \varphi} \mp (I \pm U) \frac{\partial \psi_s}{\partial \varphi} \right) \tag{A6}$$

where the I_N is the normalized intensity, the first term $I\,\partial(\psi_{P(V/U)})/\partial\varphi$ is the gradient of the spiral spatial phase distribution obtained from the Stokes parameters V and U. The term $(I \pm U)\,\partial\psi_s/\partial\varphi$ in Eqn. (A6) describes the variation of the state of polarization in space at each point in the observational plane of an asymptotic observer.

Both quantities present in Eqn. (A6) are calculated for each point in the image plane, and then the azimuthal spatial phase distribution is computed. The OAM states are identified by analyzing the asymmetry q between the height $h(m=1)$ of the $m=1$ peak with respect to that of $m=-1$, $h(m=-1)$, in the spiral spectra obtained from any given value of the rotation and inclination parameters of the KBH and characterized by the ratio $q = h(m=1)/h(m=-1)$, the parameter characterizing the OAM spectrum asymmetry and thus corresponding to the BH rotation and inclination parameters a and i. The other physical radiation emission parameters of the AD tested in our simulations spanned the photon power law index range $0.1 \leq \Gamma \leq 2$. Here we report simulations for $\Gamma = 2$, indicating a mostly thermal emission, and a radial power law index $C_r = 3$ for a radiation transfer equation with polarization, assuming a scattering dominated semi-infinite atmosphere [29]. The main results for $a = 0.9$ are reported in Fig. 3.

As has been demonstrated experimentally in the radio domain [34–36], vortex beams are detectable and can be accurately characterized with interferometric techniques. In our case, however, we employ instead a non-interferometric technique that amounts to the measurement of the vortex beam wavefront based on the Transport of Intensity Equation (TIE) and reduced error procedure [9, 37] of the four images of the Einstein ring. The EHT observations were made at 1.3 mm wavelength to generate the spatial phase distribution of the EM field and provide an estimate of the OAM spectral content in the lensed light.

In the reconstruction of the spatial phase distribution from the intensity of the field, the EM waves are described by complex-valued solutions $u(r)$ of the paraxial wave equation [37, 38]

$$\left(\boldsymbol{\nabla}_{(x,y)} \cdot \boldsymbol{\nabla}_{(x,y)} + 4\pi \mathrm{i} \frac{\partial}{\partial z} \right) u(r) = 0 \tag{A7}$$

where $\boldsymbol{\nabla}_{(x,y)}$ represents the vector nabla differential operator in the image plane (x,y) perpendicular to the z axis connecting the BH and the asymptotic observer.

By multiplying equation (A7) with its complex conjugate, one can split the equation into a system of partial differential equations describing the intensity I (the TIE equation) and the phase evolution P with respect a motion across the z axis as in Ref. 37

$$\frac{\partial I}{\partial z} = -\frac{1}{2\pi} \boldsymbol{\nabla}_{(x,y)} \cdot \left(I \boldsymbol{\nabla}_{(x,y)} P \right) \tag{A8a}$$

$$\frac{\partial P}{\partial z} = \frac{1}{4\pi\sqrt{I}} \nabla^2_{(x,y)} \sqrt{I} - |\boldsymbol{\nabla}_{(x,y)} P|^2 \tag{A8b}$$

where I is the intensity and P the phase distributions in the plane of propagation that evolves along the z coordinate. The quantity $|\boldsymbol{\nabla}_{(x,y)} P|$ is the magnitude of the phase gradient vector in the image plane.

To solve the equation system (A8) and recover the spatial phase distribution, and thus the OAM imprinted in the experimental data, we split the four observations into two subgroups of two images, each separated by the interval of one day. This was done in order to reduce any possible influence on the procedure due to possible actual physical changes in the Einstein ring for a KBH supposed to rotate near the maximum rate. We found that during these time intervals the stability of the source does not reflect dramatic structural changes, as already stated in Refs. 5 and 39. Also, the evolution of P and I along the z axis expressed in Eqns. (A8) is provided by the motion of

the Earth during the acquisitions. The TIE equation can be applied even though the shift along z due to the motion of our planet around the Sun in the interval of one day appears to be enormous with respect to the wavelength. However, this method still applies as this motion represents a fairly small fraction of the distance travelled by light from M87 to the Earth and because of the stability of propagation of the light so far observed and the slow evolution of the source during the acquisition time interval.

Appendix B: Additional material

Phase reconstruction with TIE and KERTAP-based numerical simulations

The reconstruction of the phase profile from intensity patterns of a wavefront is a novel non-interferometric technique based on the Transport of Intensity Equation (TIE) that requires a careful mathematical and numerical analysis of the problem [9, 37]. In our case we limit our analysis to paraxial optics. In principle this method only requires a field intensity acquisition system — such as the Event Horizon Telescope (EHT) — that takes snapshots at different distances, as it were mounted over an optical translation stage. This occurs naturally since Earth and M87 are in relative motion. Even if the relative motion of the source and the acquisition system is of an enormous amount of wavelengths, $\lambda = 0.0013$ m corresponding to 230 GHz, the stability of the source during the acquisition in different epochs, the stability of the signal propagation and the optimization procedure adopted in the image reconstruction to minimize the acquisition errors, and the simple geometry of the Einstein ring as observed in M87, ensure a good result allowing a determination of the spiral spectrum, and hence the rotation parameter of the black hole (BH).

To proceed with the analysis of the BH rotation we must obtain a reference OAM spectrum from numerical simulations and link the asymmetry of $m = 1$ and $m = -1$ states, that allows us to estimate, with good accuracy, the twist in the light due to the rotation of the BH. We assume that the evolution of the Einstein ring between acquisitions separated by one day can introduce small deviations in the determination of the spatial phase profile with respect to the main effect of twist of light induced by the Kerr metric lensing mechanism. The change in morphology in two different series of acquisitions of the Einstein ring separated by one day [40] due to the natural evolution of the source becomes a smaller contribution in the determination of the spiral spectrum.

The ratio between the $m = 1$ and $m = -1$ peaks in the spiral spectrum for an Einstein ring if, in the simulations, we assume a photon power law index in the range $0.1 < \Gamma < 2$, and concentrate our efforts on the canonical case [41] $\Gamma = 2$ and a radial power law index that specifies the radial steepness of the profile, of $n_r = 3$.

As a first step we use our software based on the KERTAP software [29] that describes the spacetime geometry around a rotating black hole and calculates the gravitational optics phenomena such as lensing and polarization of Kerr spacetimes [42]. We calculate the expected phase pattern of an Einstein ring for different values of the rotation parameter — the angular momentum per unit mass ($a \leq 1$) — of the BH that, together with the BH mass $m_{\rm BH}$ in Boyer–Lindquist coordinates, in geometric units ($G = c = 1$), describes the Kerr space-time with coordinates $(t, r, \vartheta, \varphi)$,

$$\mathrm{d}s^2 = \frac{\rho}{\Delta}\mathrm{d}r^2 + \rho^2 \mathrm{d}\vartheta^2 + \frac{\sin^2\vartheta}{\rho^2}\left[a\mathrm{d}t - \left(r^2 + a^2\right)\mathrm{d}\varphi\right]^2 - \frac{\Delta}{\rho^2}\left(\mathrm{d}t - a\sin^2\vartheta\mathrm{d}\varphi\right)^2 \quad \text{(B1)}$$

where

$$\rho^2 = r^2 + a^2\cos^2\vartheta \quad \text{(B2)}$$

and

$$\Delta = r^2 - 2m_{\rm BH}r + a^2 \quad \text{(B3)}$$

To obtain a more realistic result to compare with observations, we calculate the intensity pattern of the Einstein ring of a Kerr black hole (KBH), such as the one observed in M87, for different values of the rotation parameter a. In a second step, we also convolve the result provided by KERTAP with the normalized intensity patterns measured by the EHT in four different epochs, as discussed in the main text.

The propagation of the signal is quite stable also during the relative motion of the source with respect to the observer during the one day interval that separates two consecutive intensity acquisitions: the relative motion of M87 has an heliocentric radial velocity $v_{\rm rad} = 1307 \pm 7$ km/sec with a distance of $54.8 \pm 2.6 \times 10^6$ light years (ly). Even if the distance between the two wave fronts is huge in terms of wavelengths (1.3 mm), the fact that the source is stable for a time interval of one day and that the propagation is stable, one can reconstruct the wavefront even if the source and the observer are separated by a large distance. In fact, the stability in the propagation makes us conclude that the change of wavefront in one day of motion is due mainly to the phase profile of the wavefront, being the ratio between the total propagation distance and that due to the relative motion in one day

$$\frac{\Delta L_{\rm day}}{\Delta L_{\rm tot}} \approx 2.5 \times 10^{-12} \quad \text{(B4)}$$

which is very small and can only give very small perturbations to the wavefront when propagating under stable conditions [44].

Each EHT image of M87 for any epoch is obtained through the convolution of different intensity patterns by using the NMF (negative matrix factorization) reconstruction method to reduce the error in agreement with the chi-squared test ensuring a good-quality image construction process with an error of 5% in the pattern and are given in units of brightness temperature. More details are provided in the EHT scientific documentation presented and discussed in Refs. 3–6.

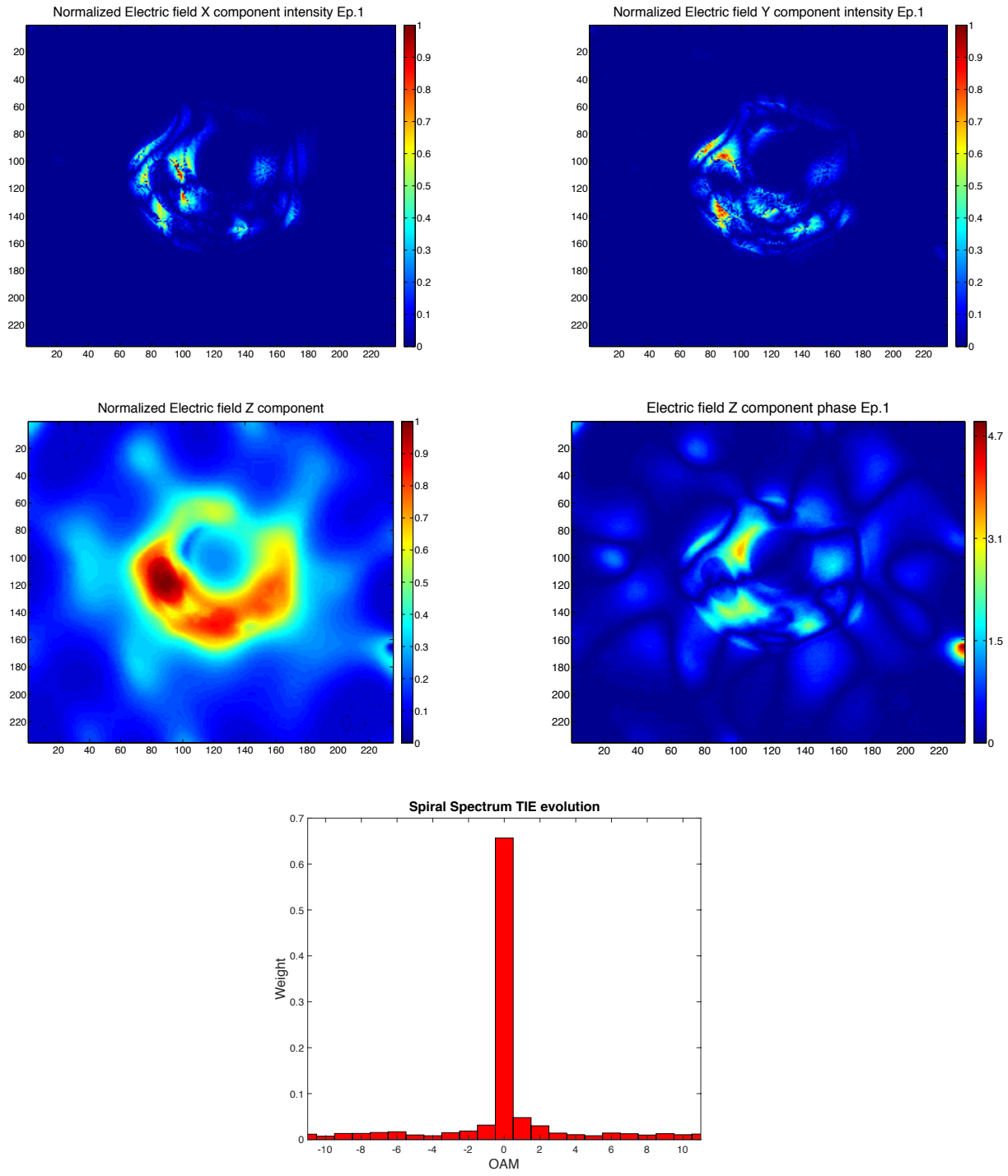

Figure 4. **Upper panels:** Normalized electric field x (left) and y component (right) reconstructed from the two EHT data acquisitions taken during epoch 1 (April 5 and 6, 2017, respectively), with the Transport of Intensity Equation (TIE) method. **Lower panels:** Normalized electric field intensity and phase across the direction of observation z and the corresponding spiral spectrum that show the presence of a black hole rotating clockwise with rotation parameter $a \sim 0.9 \pm 0.1$ and inclination 17° pointing away from Earth (see main text). The TIE reconstruction of the fields is possible because the M87 black hole Einstein ring is spatially resolved by EHT; the wavefront reconstructed here is not plane and therefore different from that emitted from a point-like source at infinity. The EM fields can be described as an unguided transverse magnetic (TM) beam in free space [43].

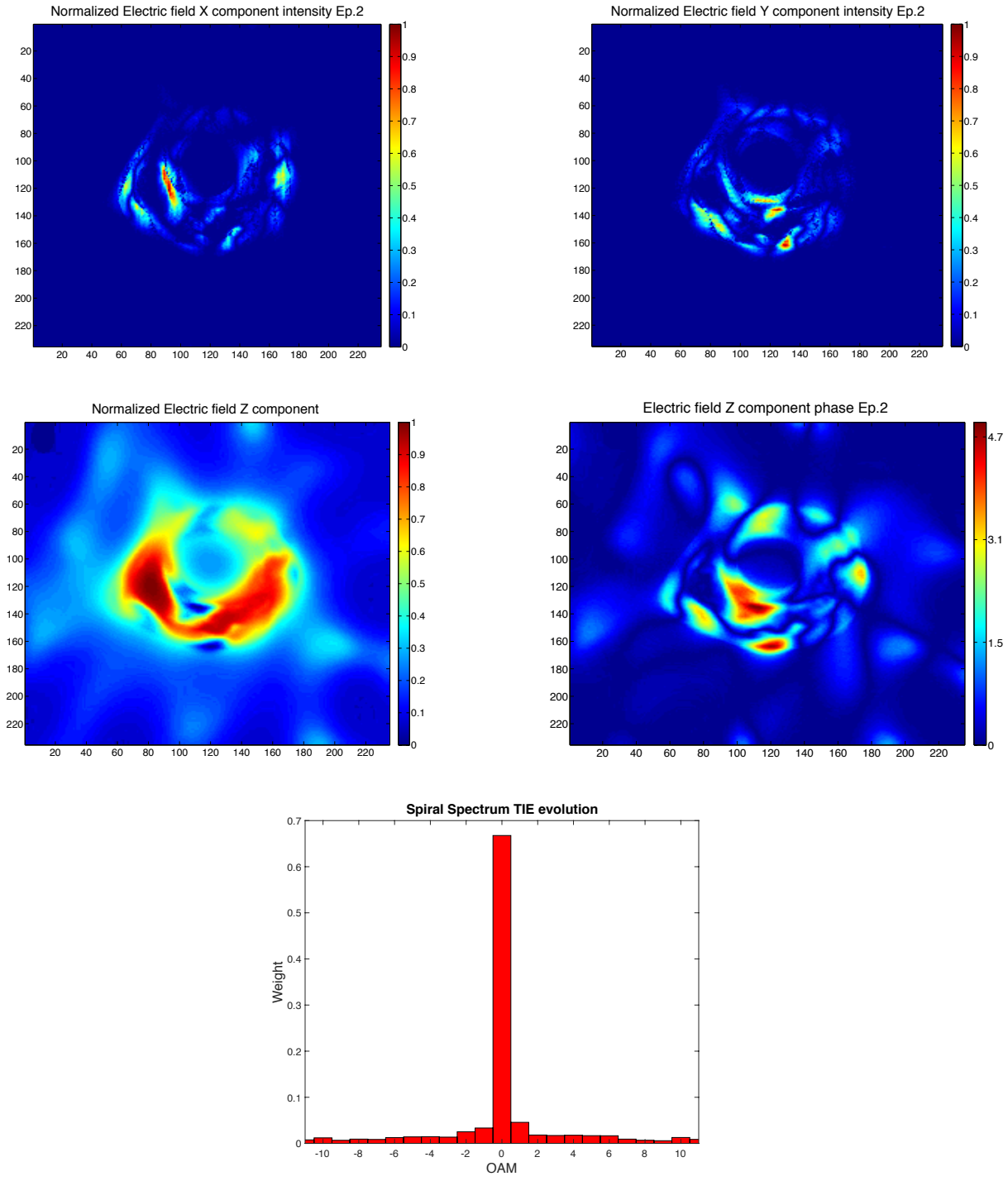

Figure 5. **Epoch 2.** Field components and spiral spectrum obtained with the TIE method, as in Fig. 4. Also here the spiral spectrum as in epoch 1 that the component of the electromagnetic field along the propagation direction to the observer, agree with the results of a twist in the light caused by a clockwise rotating black hole with rotation parameter $a \sim 0.9 \pm 0.1$ as previously discussed (see main text).

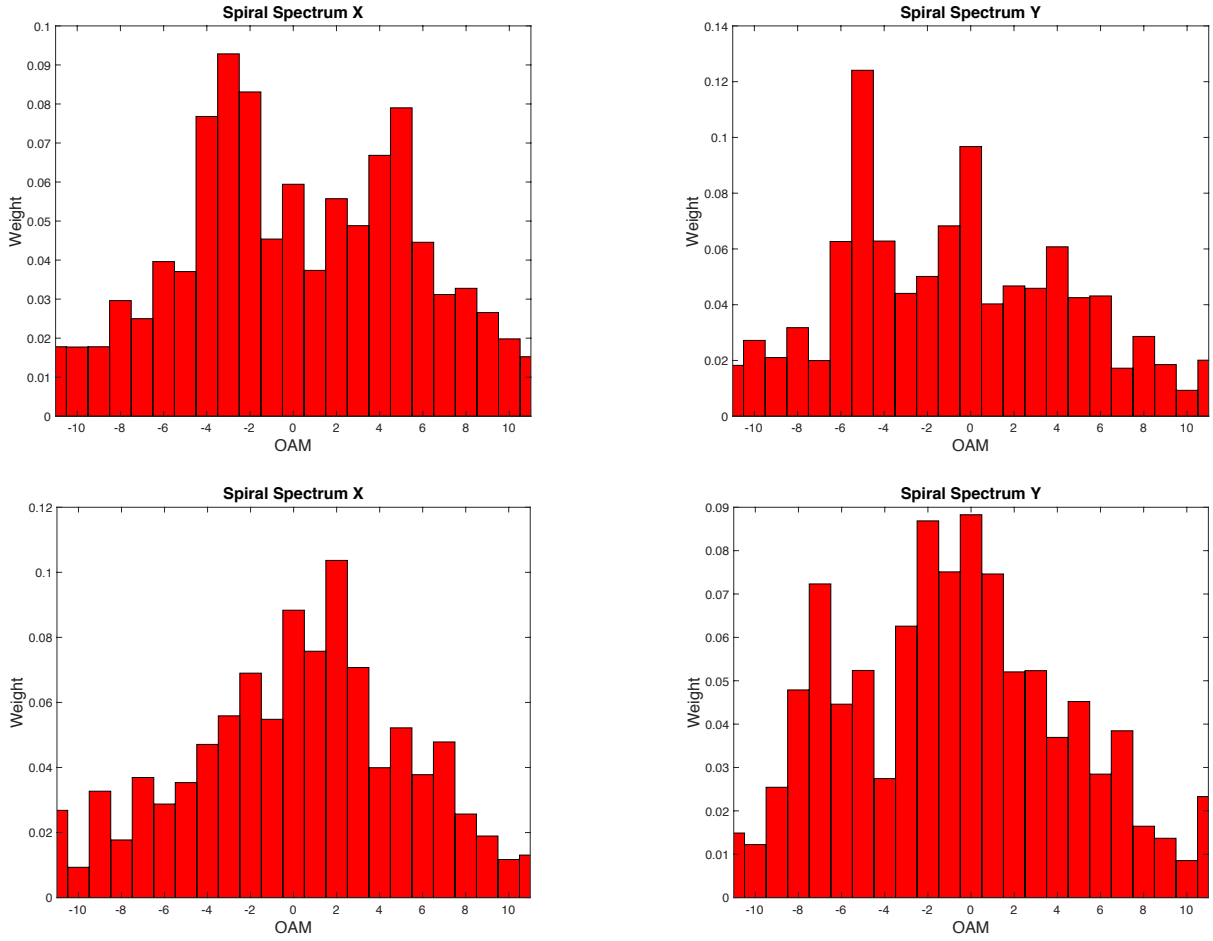

Figure 6. **Upper panel:** Spiral spectra of the x and y components of the electric field, obtained with the TIE method from EHT data in epoch 1 and those in epoch 2. **Bottom panel:** Both components in both epochs do not show a predominant OAM component, as expected.

Assuming a stable propagation and the validity of the NMR method to minimize the effects of instrumental and atmospheric effects on the wavefront, our software calculates the normalized intensity of the field obtained from the brightness temperatures of M87 EHT plots for the radiation received in the 1.3 mm band [45], solves numerically the TIE system with a finite difference method for a series of matrices (250×250) of intensity values so far obtained and then it calculates the phase profile and the spiral spectrum.

From the spatial distributions of the intensity and phase obtained (numerically) at this stage, we determine the spiral spectra and characterize the Kerr metric effect in the phase by measuring the asymmetries between the peaks $m = 1$ and $m = -1$, to be compared with those obtained from the experimental data, calculating the asymmetry parameter q. From numerical simulations we obtain a relationship between the asymmetry q and the rotation parameter a by interpolating the results present in Table I of the main text with a power law rule.

All the images provided by the EHT collaboration satisfy a 5% maximum error chi-squared test. From an error analysis, applied to the TIE equation, we obtain the total maximum error on the rotation parameter estimate $a = 0.9$ as

$$|\Delta a|_{\rm tot} = |\Delta a|_{\rm TIE} + |\Delta a|_{\rm NMF} \simeq 0.1 \qquad \text{(B5)}$$

hence yielding a first estimate of the rotation parameter at $a = 0.9 \pm 0.1$. This shows that the rotation energy [10, 46] is 10^{64} erg, which is comparable to the energy radiated by the brightest quasars over a Gyr timescale! We notice the different ratios between the $m = 0$ and $m = 1$ modes in the theoretical model and that obtained from the TIE.

From the theoretical model with a photon power law index $\Gamma = 2$ and a radial power law index $n_r = 3$, one obtains the ratio $q = h(m = 0)/h(m = 1) = 7.6$, whereas the experimental data analyzed with the TIE method we find for epoch 1 (days April 5–April 6) that the ratio $q = 14.65$ and for epoch 2 (days April 10–April 11) that the ratio $q = 13.95$. This means that the theoretical source has more coherence than that in the experimental data, even if we notice that the ratio between the two $m = 0$ and $m = 1$ modes of the experimental data are quite stable in both epochs, indicating that the TIE procedure is reliable.

The difference between the theoretical and experimental

results, excluding numerical noise, can be attributed to the concomitance of two main effects: (1) the experimental source can be more thermalized/scattered than what is assumed in the theoretical model, indicating a less coherent source; (2) if this loss of coherence depends on the time of separation between two consecutive acquisitions, it could be tuned by reducing Δt. Of course, this would also give more information about the coherence of the source emission mechanism by systematically varying Δt.

What is important is that the asymmetry between the $m = 1$ and $m = -1$ modes are stable, both in theory and experiment, suggesting that this is a promising way to directly determine the twist of spacetime and electromagnetic waves due to the rotation of the BH.

A better result could be obtained with a fast imaging technique, involving all EHT radio telescopes, allowing a series of consecutive snapshots, with a short coherence time due to atmospheric phase fluctuations that can occur on timescales of tens of seconds. This could be implemented in future EHT observations, together with the experimental acquisition of the azimuthal spatial phase profile analysis obtained with interferometric techniques centred on the BH shadow. An antenna and data acquisition system optimally designed for direct measurement of OAM would open entirely new avenues in astronomy and space sciences and technology in general.

ACKNOWLEDGMENTS

We acknowledge Guido Chincarini for his help and useful discussions. F. T. acknowledges ZKM and Peter Weibel for the financial support.

[1] Fabrizio Tamburini, Bo Thidé, Gabriel Molina-Terriza, and Gabriele Anzolin, "Twisting of light around rotating black holes," Nature Phys. **7**, 195–197 (2011).

[2] Juan P. Torres and Lluis Torner, *Twisted Photons: Applications of Light With Orbital Angular Momentum* (Wiley-Vch Verlag, John Wiley and Sons, Weinheim, DE, 2011).

[3] EHT Collaboration *et al.*, "The shadow of the supermassive black hole," Astrophys. J. Lett. **875**, L1(17) (2019), First M87 Event Horizon Telescope Results I.

[4] EHT Collaboration *et al.*, "Imaging the central supermassive black hole," Astrophys. J. Lett. **875**, L4(52) (2019), First M87 Event Horizon Telescope Results IV.

[5] EHT Collaboration *et al.*, "Physical origin of the asymmetric ring," Astrophys. J. Lett. **875**, L5(31) (2019), First M87 Event Horizon Telescope Results V.

[6] EHT Collaboration *et al.*, "The shadow and mass of the central black hole," Astrophys. J. Lett. **875**, L6(44) (2019), First M87 Event Horizon Telescope Results VI.

[7] Lluis Torner, Juan P. Torres, and Silvia Carrasco, "Digital spiral imaging," Opt. Express **13**, 873–881 (2005).

[8] Dengke Zhang, Xue Feng, Kaiyu Cui, Fang Liu, and Yidong Huang, "Identifying orbital angular momentum of vectorial vortices with Pancharatnam phase and Stokes parameters," Sci. Rep. **5**, 11982 (2015).

[9] Axel Lubk, Giulio Guzzinati, Felix Börrnert, and Jo Verbeeck, "Transport of intensity phase retrieval of arbitrary wave fields including vortices," Phys. Rev. Lett. **111**, 173902 (2013).

[10] Demetrios Christodoulou and Remo Ruffini, "Reversible transformations of a charged black hole," Phys. Rev. D **4**, 3552–3555 (1971).

[11] Jianchao Feng and Qingwen Wu, "Constraint on the black hole spin of M87 from the accretion-jet model," Mon. Not. Roy. Astron. Soc. , 612–616 (2017).

[12] Gabriele Anzolin, Fabrizio Tamburini, Antonio Bianchini, Gabriele Umbriaco, and Cesare Barbieri, "Optical vortices with starlight," Astron. Astrophys. **488**, 1159–1165 (2008).

[13] Fabrizio Tamburini, Gabriele Anzolin, G. Umbriaco, Antonio Bianchini, and Cesare Barbieri, "Overcoming the Rayleigh criterion limit with optical vortices," Phys. Rev. Lett. **97**, 163903(4) (2006).

[14] W. I. Fushchich and A. G. Nikitin, *Symmetries of Maxwell's Equations*, Mathematics and Its Applications (Soviet Series) (D. Reidel Publishing Company, Dordrecht, NL, 1987) pp. xiv+214.

[15] Fabrizio Tamburini, Mariafelicia De Laurentis, Ignazio Licata, and Bo Thidé, "Twisted soft photon hair implants on black holes," Entropy **19**, 458 (2017).

[16] M. Harwit, "Photon orbital angular momentum in astrophysics," Astrophys. J. **597**, 1266–1270 (2003).

[17] B. Thidé, Nicholas M. Elias, II, F. Tamburini, S. M. Mohammadi, and J. T. Mendonça, "Applications of electromagnetic OAM in astrophysics and space physics studies," in *Twisted Photons: Applications of Light With Orbital Angular Momentum*, edited by Juan P. Torres and Lluis Torner (Wiley-Vch Verlag, John Wiley and Sons, Weinheim, DE, 2011) Chap. 9, pp. 155–178.

[18] Alois Mair, Alipasha Vaziri, Gregor Weihs, and Anton Zeilinger, "Entanglement of the orbital angular momentum states of photons," Nature **412**, 313–316 (2001).

[19] Jonathan Leach, Miles J. Padgett, Stephen M. Barnett, Sonja Franke-Arnold, and Johannes Courtial, "Measuring the orbital angular momentum of a single photon," Phys. Rev. Lett. **88**, 257901(4) (2002).

[20] F. Tamburini and D. Vicino, "Photon wave function: A covariant formulation and equivalence with QED," Phys. Rev. A **78**, 052116(5) (2008).

[21] G. F. Calvo, A. Picón, and E. Bagan, "Quantum field theory of photons with orbital angular momentum," Phys. Rev. A **73**, 013805–1 (2006).

[22] Gabriel Molina-Terriza, Juan P. Torres, and Lluis Torner, "Twisted photons," Nature Phys. **3**, 305–310 (2007).

[23] Kris Beckwith and Chris Done, "Extreme gravitational lensing near rotating black holes," Mon. Not. Roy. Astron. Soc. **359**, 1217–1228 (2005).

[24] F. S. Su and R. L. Mallett, "The effect of the Kerr metric on the plane of polarization of an electromagnetic wave," Astrophys. J. **238**, 1111–1125 (1980).

[25] H. Dehnen, "Gravitational Faraday-effect," Int. J. Theor. Phys. **7**, 467–474 (1973).

[26] Piero Carini, Long-Long Geng, Miao Li, and Remo Ruffini, "Phase evolution of the photon in Kerr spacetime," Phys. Rev. D **46**, 5407–5410 (1992).

[27] Long-Long Feng and Wolung Lee, "Gravitomagnetism and the Berry phase of photon in an rotating gravitational field," Int.

J. Mod. Phys. D. **10**, 961–969 (2001).

[28] Huan Yang and Marc Casals, "Wavefront twisting by rotating black holes: Orbital angular momentum generation and phase coherent detection," Phys. Rev. D **90**, 023014 (2014).

[29] Bin Chen, Ronald Kantowski, Xinyu Dai, Eddie Baron, and Prasad Maddumage, "Algorithms and programs for strong gravitational lensing in Kerr space-time including polarization," Astrophys. J. Suppl. Ser. **218**, 4 (2015).

[30] Akihiro Doi, Kazuhiro Hada, Hiroshi Nagai, Motoki Kino, Mareki Honma, Kazunori Akiyama, Tomoaki Oyama, and Yusuke Kono, "ALMA continuum spectrum of the M87 nucleus - quasi-simultaneous continuum observations at bands-3, 6, 7, and 9," EPJ Web of Conferences **61**, 08008 (2013).

[31] B. Thidé, F. Tamburini, H. Then, C. G. Someda, and R. A. Ravanelli, "The physics of angular momentum radio," arXiv.org , 34 (2014), arXiv:1410.4268 [physics.optics].

[32] Stephen M. Barnett and L. Allen, "Orbital angular momentum and nonparaxial light beams," Opt. Commun. **110**, 670–678 (1994).

[33] Les Allen and Miles Padgett, "The orbital angular momentum of light: An introduction," in *Twisted Photons: Applications of Light With Orbital Angular Momentum*, edited by Juan P. Torres and Lluis Torner (Wiley-Vch Verlag, John Wiley and Sons, Weinheim, DE, 2011) Chap. 1, pp. 1–12.

[34] B. Thidé, H. Then, J. Sjöholm, K. Palmer, J. Bergman, T. D. Carozzi, Ya. N. Istomin, N. H. Ibragimov, and R. Khamitova, "Utilization of photon orbital angular momentum in the low-frequency radio domain," Phys. Rev. Lett. **99**, 087701(4) (2007).

[35] Fabrizio Tamburini, Elettra Mari, Bo Thidé, Cesare Barbieri, and Filippo Romanato, "Experimental verification of photon angular momentum and vorticity with radio techniques," Appl. Phys. Lett. **99**, 204102 (2011).

[36] Fabrizio Tamburini, Elettra Mari, Anna Sponselli, Bo Thidé, Antonio Bianchini, and Filippo Romanato, "Encoding many channels on the same frequency through radio vorticity: first experimental test," New J. Phys. **14**, 03301 (2012).

[37] Adrián Ruelas, Servando Lopez-Aguayo, and Julio C. Gutiérrez-Vega, "Wavefront reconstruction of vortex beams via a simplified transport of intensity equation and its symmetry based error reduction," J. Opt. **21**, 015602 (2018).

[38] Joseph W. Goodman, *Introduction to Fourier Optics*, 3rd ed. (Roberts, Englewood, CO, USA, 1996) p. 528.

[39] Sheperd S. Doeleman, Vincent L. Fish, David E. Schenck, Christopher Beaudoin, Ray Blundell, Geoffrey C. Bower, Avery E. Broderick, Richard Chamberlin, Robert Freund, Per Friberg, Mark A. Gurwell, Paul T. P. Ho, Mareki Honma, Makoto Inoue, Thomas P. Krichbaum, James Lamb, Abraham Loeb, Colin Lonsdale, Daniel P. Marrone, James M. Moran, Tomoaki Oyama, Richard Plambeck, Rurik A. Primiani, Alan E. E. Rogers, Daniel L. Smythe, Jason SooHoo, Peter Strittmatter, Remo P. J. Tilanus, Michael Titus, Jonathan Weintroub, Melvyn Wright, Ken H. Young, and Lucy M. Ziurys, "Jet-launching structure resolved near the supermassive black hole in M87," Science **338**, 355–358 (2012).

[40] One day is the separation between two consecutive acquisitions of a set of images that are used to build up the pertinent image for that specific epoch.

[41] Heino Falcke and Peter L. Biermann, "The jet-disk symbiosis I. radio to X-ray emission models for quasars," Astron. Astrophys. **293**, 665–682 (1995).

[42] Roy P. Kerr, "Gravitational field of a spinning mass as an example of algebraically special metrics," Phys. Rev. Lett. **11**, 237–238 (1963).

[43] Lawrence W. Davis and George Patsakos, "TM and TE electromagnetic beams in free space," Opt. Lett. **6**, 22–23 (1981).

[44] F. Tamburini, C. Cuofano, M. Della Valle, and R. Gilmozzi, "No quantum gravity signature from the farthest quasars," Astron. Astrophys. **533**, A71 (2011).

[45] George B. Rybicki and Alan P. Lightman, *Radiative Processes in Astrophysics*, Physics Textbook (Wiley, Weinheim, 2004) p. 382.

[46] David L. Wiltshire, Matt Visser, and Susan M. Scott, eds., *The Kerr Spacetime: Rotating Black Holes in General Relativity*, 1st ed. (Cambridge University Press, Cambridge, UK ; New York, 2009).